Electromagnetically induced frame dragging around astrophysical objects

Andrés F. Gutiérrez-Ruiz[*] and Leonardo A. Pachón[†]

Grupo de Física Atómica y Molecular, Instituto de Física, Facultad de Ciencias Exactas y Naturales, Universidad de Antioquia UdeA; Calle 70 No. 52-21, Medellín, Colombia

(Received 13 April 2015; published 15 June 2015)

Frame dragging (Lense-Thirring effect) is generally associated with rotating astrophysical objects. However, it can also be generated by electromagnetic fields if electric and magnetic fields are simultaneously present. In most models of astrophysical objects, macroscopic charge neutrality is assumed and the entire electromagnetic field is characterized in terms of a magnetic dipole component. Hence, the purely electromagnetic contribution to the frame dragging vanishes. However, strange stars may possess independent electric dipole and neutron stars independent electric quadrupole moments that may lead to the presence of purely electromagnetic contributions to the frame dragging. Moreover, recent observations have shown that in stars with strong electromagnetic fields, the magnetic quadrupole may have a significant contribution to the dynamics of stellar processes. As an attempt to characterize and quantify the effect of electromagnetic frame dragging in these kinds of astrophysical objects, an analytic solution to the Einstein-Maxwell equations is constructed here on the basis that the electromagnetic field is generated by the combination of arbitrary magnetic and electric dipoles plus arbitrary magnetic and electric quadrupole moments. The effect of each multipole contribution on the vorticity scalar and the Poynting vector is described in detail. Corrections on important quantities such the innermost stable circular orbit (ISCO) and the epicyclic frequencies are also considered.

DOI: 10.1103/PhysRevD.91.124047 PACS numbers: 04.40.Nr, 04.20.Cv, 04.40.Dg, 95.30.Sf

I. INTRODUCTION

Frame dragging (Lense-Thirring effect) is the quintessential hallmark of general relativity and is the result of the spacetime vorticity. It was detected by the Gravity Probe B [1] and traditionally, it has been associated with rotating stellar astrophysical objects and in other astrophysical contexts, such as galactic models, the frame dragging has been associated to the presence of magnetogravitational monopoles [2,3]. Surprisingly, if the astrophysical object does not rotate but possesses both electric and magnetic fields, the spacetime vorticity does not vanish [4–6]. In this case, frame dragging is of purely electromagnetic nature and it is associated with the existence of a nonvanishing electromagnetic Poynting vector around the source [5–9].

In most of the early models of astrophysical objects, macroscopic charge neutrality is assumed [10] and the magnetic field is characterized in terms of a pure dipole component [11–14]. This idea was endorsed by the confirmation of many predicted features of a star with a dipole field using two- and three-dimensional magnetohydrodynamic numerical simulations of magnetospheric accretion [15–18]. Thus, under this configuration the *purely* electromagnetic contribution to the vorticity tensor vanishes. However, astrophysical objects such as strange stars may possess independent electric dipole (see Sec. 10.4 in Ref. [19]) and neutron stars independent electric quadrupole moments (see below), which may lead to the presence of purely electromagnetic contributions to frame dragging. A precise account of those contributions is not available because of the lack of an analytic exact solution with such a complex electromagnetic field configuration.

Moreover, recent observations have shown that in stars with strong electromagnetic fields, the magnetic quadrupole may have significant contributions on the dynamics of stellar processes. Therefore, it is well known by now that the actual configuration of the magnetic field of strongly magnetized stars may depart from the dipole configuration [20]. As an attempt to describe the spacetime geometry surrounding these kinds of astrophysical objects, an analytic solution to the Einstein-Maxwell field equations is constructed here on the basis that the electromagnetic field is generated by the combination of arbitrary magnetic and electric dipoles plus arbitrary magnetic and electric quadrupole moments. This analytic exact solution allows for analyzing, e.g., the effect of each multipole contribution on the vorticity scalar and the Poynting vector (see Sec. V). Moreover, it is possible to predict corrections to important quantities such as the innermost stable circular orbit and the epicyclic frequencies.

To motivate further the derivation of the model considered here, the observational evidence for the existence of nondipolar fields in a variety of astrophysical objects is discussed next.

[*]afelipe.gutierrez@udea.edu.co
[†]leonardo.pachon@udea.edu.co

 © 2015 American Physical Society

II. OBSERVATIONAL EVIDENCE OF NONDIPOLAR FIELDS

Measurements of magnetic fields of strongly magnetized stars, based on the Zeeman-Doppler imaging technique [21], have shown that for these kinds of astrophysical objects the magnetic field has a complicated multipolar topology in the vicinity of the star [22–26]. This feature certainly is of prime relevance in, e.g., the accretion-disk dynamics in binary systems because if the quadrupole component dominates, then the flow of matter into the star will certainly differ from the well-known dynamics induced by a pure dipole field [25].

Complex configurations of magnetic fields are also present in stars such as the T-Tauri stars. They are young stellar objects of low mass that present variations in their luminosity. An important subclass of this kind of star is the so-called classical T-Tauri stars (cTTS) because they present accretion from the circumstellar disk [27]. Recent evidence points out that in classical T-Tauri stars, the magnetic field near the star is strongly nondipolar [26]. In the particular case of V2129 Oph, there exits a dominant octupole, 0.12 T, and a weak dipole component, 0.035 T, of the magnetic field [28]. Understanding the circumstellar disk dynamics, under complex field topologies, could provide insight into the formation of planets and the evolution of the star itself.

The discussion above also applies to white dwarfs. The first observations indicated that only a small fraction of white dwarfs appear to exhibit magnetic fields. However, the observational situation changed significantly by the discovery of strong-field magnetic white dwarfs [29–31], which are known to cover a wide range of field strengths ~1–100 T and deviates from the simple dipolar configuration [32,33]. Recent spectropolarimetric observations in white dwarf have shown that, in addition to the dipole term, the quadrupole and octupole terms make significant contributions to the field when it is represented as an axisymmetric multipolar expansion [34]. Many studied cases indicate that higher multipole components or nonaxisymmetric components may be required in a realistic model of white dwarfs (see, e.g., Ref. [35]).

Magnetars constitute an additional source of motivation. They are characterized by their extremely powerful magnetic fields, covering strengths from $\sim 10^8$ to $\sim 10^{11}$ T [36,37], so that they can have occasional violent bursts. However, certain magnetars, such as the SGR $0418+5729$, undergo this bursting phenomenon even with weak magnetic fields ($\sim 10^8$ T) [38]. For SGR $0418+5729$, the observed x-ray spectra cannot be fit with this low field strength; hence, it has been suggested that a hidden nondipole field component must be present to explain the bursting episodes [39].

In summary, there is sufficient observational evidence to develop a consistent analytic closed representation of the exterior spacetime around stars with nondipolar magnetic fields.

III. ANALYTIC FORMULAS OF THE MODEL

By combining the facts that (i) almost all the analytic closed form models for relevant astrophysical objects have been conceived in the frame of stationary axisymmetry geometry (see [40–45] for the case of neutron stars); (ii) powerful tools to construct the exact solution to the Einstein-Maxwell field equation have been developed, e.g. [46–48]; and (iii) systematic studies on the construction of the exact solution from its physical content have been performed [49,50], a new analytic exact solution to the Einstein-Maxwell field equations is introduced below. This solution provides physical insight, e.g., into the influence of high order electromagnetic multipole moments in the frame dragging and in studying quasiperiodic oscillations (QPOs), which become a useful tool to identify the characteristics of the compact objects present in low mass x-ray binaries (LMXBs) [51–53]. The model presented here is a member of the N-solitonic solution derived in Ref. [54]. In Appendix A the relevant equations of the derived metric are summarized.

In terms of the quasicylindrical Weyl-Lewis-Papapetrou coordinates $x^\mu = (t, \rho, z, \phi)$, the simplest form of the line element for the stationary axisymmetric case was given by Papapetrou [55],

$$ds^2 = g_{\mu\nu} dx^\mu dx^\nu, \tag{1}$$

with $g_{tt} = -f(\rho, z)$, $g_{t\phi} = f(\rho, z)\omega(\rho, z)$, $g_{\phi\phi} = \rho^2 f^{-1}(\rho, z) - f(\rho, z)\omega^2(\rho, z)$, and $g_{zz} = g_{\rho\rho} = e^{2\gamma(\rho,z)} f^{-1}(\rho, z)$. The metric functions f, ω, and γ can be obtained from the Ernst complex potentials $\mathcal{E}$ and Φ (see details in Ref. [46]). The Ernst potentials obey the relations [46]

$$\begin{aligned}(\mathrm{Re}\mathcal{E} + |\Phi|^2)\nabla^2\mathcal{E} &= (\nabla\mathcal{E} + 2\Phi^*\nabla\Phi)\cdot\nabla\mathcal{E},\\ (\mathrm{Re}\mathcal{E} + |\Phi|^2)\nabla^2\Phi &= (\nabla\mathcal{E} + 2\Phi^*\nabla\Phi)\cdot\nabla\Phi.\end{aligned} \tag{2}$$

From a physical viewpoint, the Ernst potentials are relevant because they lead to the definition of the analogues of the Newtonian gravitational potential, $\xi = (1-\mathcal{E})/(1+\mathcal{E})$, and the Coulomb potential, $q = 2\Phi/(1+\mathcal{E})$. The real part of ξ accounts for the matter distribution and its imaginary part for the mass currents. Also, the real part of the q potential denotes the electric field and its imaginary part the magnetic field.

The Ernst equations (2) can be solved by means of Sibgatullin's integral method [47,48], according to which the complex potentials $\mathcal{E}$ and Φ can be calculated from specified axis data $\mathcal{E}(z, \rho = 0)$ and $\Phi(z, \rho = 0)$ [47,48]. Motivated by the accuracy [41,42] and the level of generality of the analytic solution derived in Ref. [42], the Ernst potential $\mathcal{E}(z, \rho = 0)$ is chosen as in Ref. [42]. To construct the exact solution that represents the electromagnetic field configuration described above, the Ernst potential $\Phi(z, \rho = 0)$ is chosen following the prescription in Ref. [49]. The Ernst potentials on the symmetry axis read

$$\mathcal{E}(z,\rho=0)=\frac{z^3-z^2(m+ia)-kz+is}{z^3+z^2(m-ia)-kz+is},$$
$$\Phi(z,\rho=0)=\frac{z^2\varsigma+z(\upsilon+i\mu)+i\zeta+\chi}{z^3+z^2(m-ia)-kz+is}. \quad (3)$$

The physical meaning of the parameters in Eq. (3) is derived from the multipole moments calculated using the Fodor-Hoenselaers-Perjés procedure [56] (see also Ref. [57]). For the present case,

$$P_0=m,\qquad P_1=iam,\qquad P_2=(k-a^2)m,\qquad P_3=-im(a^3-2ak+s),$$
$$P_4=\frac{1}{70}m[70a^4-210a^2k+13a\varsigma(\mu-i\upsilon)+140as+10k(7k-m^2+\varsigma^2)+3(\mu^2+\upsilon^2)],$$
$$P_5=-\frac{1}{21}im\{-21a^5+84a^3k+a^2(-6\mu\varsigma-63s+6i\upsilon\varsigma)+a[-63k^2+6k(m-\varsigma)(m+\varsigma)+\mu^2+5i\zeta\varsigma+\upsilon^2+5\chi\varsigma]$$
$$+k(3\mu\varsigma+42s-i\upsilon\varsigma)+2i(\mu\zeta+\upsilon\chi)+7s(\varsigma^2-m^2)\}, \quad (4)$$

$$Q_0=\varsigma,\qquad Q_1=\upsilon+i(a\varsigma+\mu),\qquad Q_2=-a^2\varsigma-a\mu+k\varsigma+\chi+i(a\upsilon+\zeta),$$
$$Q_3=-a^2\upsilon-a\zeta+k\upsilon+i(-a^3\varsigma-a^2\mu+a(2k\varsigma+\chi)+k\mu-s\varsigma),$$
$$Q_4=a^4\varsigma+a^3(\mu-i\upsilon)+a^2(-3k\varsigma-i\zeta-\chi)+\frac{1}{70}a[140s\varsigma-(\mu-i\upsilon)(140k-3m^2-10\varsigma^2)]$$
$$+\frac{1}{7}\{\varsigma[\varsigma(k\varsigma+i\zeta+\chi)+(\mu-i\upsilon)^2]+(7k-m^2)(k\varsigma+i\zeta+\chi)+7s(\mu-i\upsilon)\},$$
$$Q_5=\frac{1}{21}\{21ia^5\varsigma+21a^4(\upsilon+i\mu)-21ia^3(4k\varsigma+i\zeta+\chi)+a^2[63is\varsigma-i(63k+8\varsigma^2)(\mu-i\upsilon)]$$
$$+ia\{-\varsigma[\varsigma(8k\varsigma+i\zeta+\chi)+9\mu^2-16i\mu\upsilon-7\upsilon^2]+(21k-2m^2)(3k\varsigma+2i\zeta+2\chi)$$
$$+42s(\mu-i\upsilon)\}-i(\mu-i\upsilon)(-21k^2+2km^2+\mu^2+\upsilon^2)+k\varsigma^2(\upsilon-i\mu)$$
$$+\varsigma(-42iks-6\mu\zeta+6i\mu\chi+7im^2s+8i\zeta\upsilon+8\upsilon\chi)+21s(\zeta-i\chi)+7is\varsigma^3\}. \quad (5)$$

Specifically, the interpretation of the parameters based on the multipole expansion in Eqs. (4) and (5) is as follows. The real parameter m corresponds to the total mass, and a to the total angular moment per unit mass while k and s are related to the mass-quadrupole moment and the differential rotations, respectively. For later convenience, an electric monopole contribution Q_0, characterized by the parameter ς, was introduced above. Parameters υ and μ are associated with the electric and magnetic dipole moments, respectively, whereas χ and ζ with the electric and magnetic quadrupole moments, respectively. The existence of an electric dipole is theorized for strange stars (see Ref. [58]). A summary of the arbitrary parameters and the multipole moments they are related to can be found in Table I.

The mass moment P_2 governs the deformation of the star and it is composed of two parts: the term a^2m that is the usual rotation-induced deformation and a second contribution km that accounts for a possible intrinsic deformation of the star [59,60]. An analogous argument can be formulated in the case of the electric moments. The real part of Q_2 accounts for the electric quadrupole contribution to the total electromagnetic quadrupole moment. The terms $-a^2\varsigma$ and $-a\mu$ account for the rotation-induced redistribution of the electric charge and deformation of the magnetic dipole, whereas the term $k\varsigma$ accounts for the contribution from the charge distributed over the intrinsic deformed mass. The additional parameter χ is added to account for any additional possible contribution to the total quadrupole moment.

The multipole expansion in Eq. (5) shows that even if the magnetic dipole parameter is zero ($\mu=0$), a magnetic dipole component (imaginary part of Q_1) is present provided by the rotation of the electric charge Q_0. Similarly, even if the magnetic quadropole parameter ζ is set to zero, a rotating electric dipole can induce a magnetic quadrupole (imaginary part of Q_2). For the electric part of the multipole expansion in Eq. (5), an analogous behavior is observed; namely, a rotating magnetic dipole can induce an electric quadrupole moment and

TABLE I. Summary of the electromagnetic parameters and the multipole moments they are related to.

Symbol	Associated multipole moment
ς	Electric monopole
υ	Electric dipole
χ	Electric quadrupole
μ	Magnetic dipole
ζ	Magnetic quadrupole

a rotating magnetic quadrupole can generate an electric octupole moment. Based on these processes, the astrophysical source can afford a nonvanishing induced Poynting vector and, correspondingly, an induced nonvanishing flux of electromagnetic energy around the source that will contribute to the frame dragging induced solely by the mass currents.

IV. CHARACTERIZATION OF THE ELECTROMAGNETIC FIELDS

To describe the electromagnetic properties of the solution, the electric and magnetic fields, in the spacetime surrounding the star, are calculated by means of the expressions

$$E_\alpha = F_{\alpha\beta}u^\beta, \qquad B_\alpha = -\frac{1}{2}\epsilon_{\alpha\beta}{}^{\gamma\delta}F_{\gamma\delta}u^\beta, \tag{6}$$

where $F_{\alpha\beta}$ is the electromagnetic field tensor $F_{\alpha\beta} = 2A_{[\beta;\alpha]}$, $A_\mu = (0, 0, A_\phi, -A_t)$ is the electromagnetic four-potential, u_α is a timelike vector and $\epsilon_{\alpha\beta\gamma\delta}$ is the totally antisymmetric tensor of positive orientation with norm $\epsilon_{\alpha\beta\gamma\delta}\epsilon^{\alpha\beta\gamma\delta} = -24$ [61]. For a congruence of observers at rest in the frame of (1), the four-velocity is defined by the timelike vector $u^\alpha = (1/\sqrt{f}, 0, 0, 0)$. The vectorial fields have components in the ρ and z directions only. The components of the electric field are given by

$$E_\rho = -\frac{\sqrt{f}}{e^{2\gamma}}A_{t,\rho}, \qquad E_z = -\frac{\sqrt{f}}{e^{2\gamma}}A_{t,z}, \tag{7}$$

and for the magnetic field by

$$B_\rho = \frac{f^{3/2}}{\rho e^{2\gamma}}(-\omega A_{t,z} + A_{\phi,z}), \tag{8}$$

$$B_z = -\frac{f^{3/2}}{\rho e^{2\gamma}}(-\omega A_{t,\rho} + A_{\phi,\rho}). \tag{9}$$

The explicit form of the fields can be found in Appendix B.

Figure 1 shows the force lines of the magnetic field for various values of the magnetic quadrupole parameter ζ and for realistic values of the mass and mass current multipoles. Specifically, the vacuum multipole moments of the solution mass, angular moment, mass quadrupole and current octupole have been fixed to the numerical ones obtained in Ref. [62]. They are listed in Table II. In particular, for Fig. 1(a), $\zeta = 0$ km^3; for 1(b), $\zeta = 10$ km^3; for 1(c), $\zeta = 25$ km^3 and for 1(d), $\zeta = 50$ km^3. The increasing of the separation between consecutive force lines indicates that the magnetic field decreases while the distance increases. Figure 1 not only shows how the reflection symmetry around the plane $z = 0$ is broken because of the magnetic quadrupole [6], but also shows that at large distances from the source, the magnetic field behaves like a magnetic dipole despite the presence of strong nondipolar contributions.

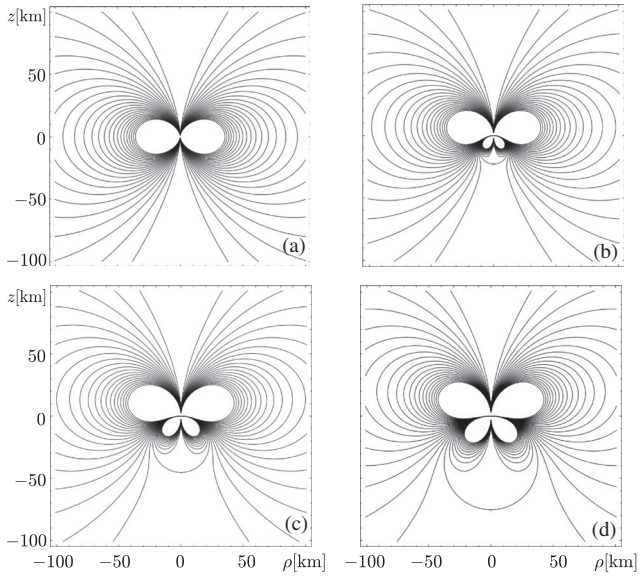

FIG. 1. Magnetic field force lines for $m = 2.071$ km, $j = 0.194$, $Q = -2.76$ km^3, $s = -2.28$ km^4, $\varsigma = 0$ km, $\upsilon = 0$ km^2, $\chi = 0$, $\mu = 1$ km^2 for (a) $\zeta = 0$ km^3, (b) $\zeta = 15$ km^3, (c) $\zeta = 30$ km^3 and (d) $\zeta = 50$ km^3. The nonelectromagnetic parameters correspond to the model 2 for the equation of state L in Ref. [62] (see also Table II).

Figure 2 shows the force lines of the electric field for a variety of values of the electric quadrupole for realistic values of the mass and mass current multipoles listed in Table II. Specifically, for Fig. 2(a), $\chi = 0$ km^3; for 2(b), $\chi = 10$ km^3; for 2(c), $\chi = 25$ km^3 and for 2(d), $\chi = 50$ km^3. As above, it is clear that reflection symmetry is broken and that at large distances the electric dipole component dominates the field configuration.

In general, the electromagnetic field of astrophysical objects is expected to be a combination of the results depicted in Figs. 1 and 2. Moreover, as shown below, the breaking of the reflection symmetry has an important role on the vorticity of the spacetime. After characterizing the electromagnetic fields, the generation of purely electromagnetic frame dragging is discussed below.

TABLE II. Realistic numerical solutions for rotating neutron stars derived by Pappas and Apostolatos [62] for the equation of state L. Here, m is the total mass of the star, j is the dimensionless spin parameter where $j = J/M^2$ (J being the angular momentum), Q is the quadrupole moment and s is the current octupole moment. See Table VI of [62].

Model	m (km)	j	Q (km^3)	s (km^4)
M2	2.071	0.194	−2.76	−2.28
M3	2.075	0.324	−7.55	−10.5
M4	2.080	0.417	−12.2	−22.0
M5	2.083	0.483	−16.2	−33.9

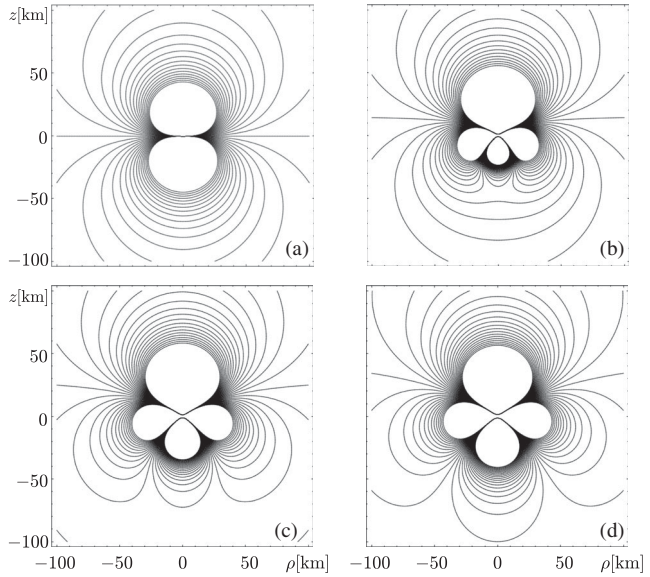

FIG. 2. Electric field force lines for $m = 2.071$ km, $j = 0.194$, $Q = -2.76$ km^3, $s = -2.28$ km^4, $\varsigma = 0$ km, $\upsilon = 1$ km^2, $\mu = 0$ km^2, $\zeta = 0$ for (a) $\chi = 0$ km^3, (b) $\chi = 10$ km^3, (c) $\chi = 25$ km^3 and (d) $\chi = 50$ km^3.

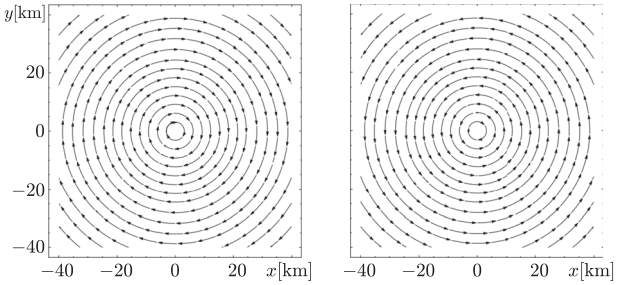

FIG. 3. Vector field of the Poynting vector for the star model $m = 2.071$ km, $j = 0.194$, $Q = -2.76$ km^3, $s = -2.28$ km^4. The electromagnetic multipoles were chosen zero except $\varsigma = 0.1$ km, $\mu = 1$ km^2 in the left panel and $\mu = -1$ km^2 in the right panel. The direction of the Poynting vector is due to the sign change in the multipole expansions in Eq. (5). Figures are presented in the quasi-Cartesian auxiliary coordinates $r \to \sqrt{x^2 + y^2}$ and $\phi = \arctan(y/x)$.

V. VORTICITY SCALAR AND POYNTING VECTOR

The physics of the frame dragging states that the rotation of the source induces a twist in the neighborhood that drags any frame of reference near the source. In the case of spacetimes endowed by complex electromagnetic fields and mass currents, frame dragging originates from a combination of the vorticity of the electromagnetic field and the vorticity associated with the mass currents.

Poynting vector.—The Poynting vector $\mathbf{S}$ carries the information about the electromagnetic energy flux in the spacetime. Because of the axially symmetric character of the spacetime, only the component along the unitary vector $\hat{\mathrm{e}}_\phi$ survives [6]. In terms of the Ernst potentials $S^\phi = \sqrt{f}\mathrm{Im}(\Phi^*_{,\rho}\Phi_{,z})/(4\pi\rho e^{2\gamma})$ [63] or more conveniently

$$S^\phi = \frac{\sqrt{f}}{8\pi\rho e^{2\gamma}}\nabla\Phi^* \times \nabla\Phi, \tag{10}$$

where it is clear that S^ϕ vanishes if Φ is purely real, purely imaginary or when their real and imaginary parts are proportional to each other. Due to the complex combination of the electromagnetic moments with the mass currents, their effects on the Poynting vector (and subsequently to the vorticity) are often subtle. However, the multipole expansion in Eq. (5) allows for a detailed description of each contribution. For instance, if $\upsilon = 0$, $\chi = 0$ and $|a\varsigma| < |\mu|$, it is then clear that, to leading order, a sign change in the magnetic dipole moment parameter μ changes the sign of the magnetic field. This has the effect of changing the rotation direction of the Poynting vector (see Fig. 3) and as discussed below, it could decrease the total vorticity of the spacetime. Figure 3 depicts the Poynting vector circulation around the source, when μ is chosen parallel (left panel) and antiparallel (right panel) to the star's rotation axis.

The change of the circulation of the Poynting vector can be understood from the potential $q(\rho, z)$ that is analogous to the Coloumb potential (see above). Under the condition that the reflection symmetry is not broken, $\upsilon = 0$ and $\zeta = 0$, a sign change of the magnetic dipole parameter μ is equivalent to changing the sign of the coordinate z with a global minus sign, namely, $q(\rho, z; \upsilon = 0, \zeta = 0, -\mu) = -q(\rho, -z; \upsilon = 0, \zeta = 0, \mu) = -q^*(\rho, z; \upsilon = 0, \zeta = 0, \mu)$. Therefore, under the conditions that reflection symmetry imposes [49], all the electric field moments change sign and this leads to a global sign of the Poynting vector.

Vorticity scalar.—For an observer at rest with respect to (1), the vorticity tensor is defined by $\omega_{\alpha\beta} = u_{[\alpha;\beta]} + \dot{u}_{[\alpha}u_{\beta]}$.

The direct calculation of $\omega_{\alpha\beta}$ for (1) yields to [6]

$$\omega_{\alpha\beta} = \begin{pmatrix} 0 & 0 & 0 & 0 \\ 0 & 0 & 0 & -\frac{1}{2}\sqrt{f}\omega_{,\rho} \\ 0 & 0 & 0 & -\frac{1}{2}\sqrt{f}\omega_{,z} \\ 0 & \frac{1}{2}\sqrt{f}\omega_{,\rho} & \frac{1}{2}\sqrt{f}\omega_{,z} & 0 \end{pmatrix}. \tag{11}$$

To quantify the vorticity, it is convenient to introduce the vorticity scalar that is defined by the contraction of the vorticity tensor and reads

$$\omega_{\mathrm{v}} = (\omega^\alpha_\beta\omega^\beta_\alpha)^{\frac{1}{2}} = f\sqrt{f(\omega^2_{,\rho} + \omega^2_{,z})}/\sqrt{2e^{2\gamma}\rho^2}, \tag{12}$$

with $\omega_{,\rho} = -\rho f^{-2}\Im(\mathcal{E}_{,z} + 2\Phi^*\Phi_{,z})$ and $\omega_{,z} = \rho f^{-2}\times \Im(\mathcal{E}_{,\rho} + 2\Phi^*\Phi_{,\rho})$. More explicitly, it reads

$$\omega_{\rm v} = \frac{e^{-\gamma}}{\sqrt{2f}} \sqrt{\Im[\mathcal{E}_{,z} + 2\Phi^*\Phi_{,z}]^2 + \Im[\mathcal{E}_{,\rho} + 2\Phi^*\Phi_{,\rho}]^2}. \quad (13)$$

The vorticity scalar can be understood in terms of its fluid mechanics analogue. It represents the rotation of the fluid. In the general relativistic case, it can be related to the rotation velocity of a family of congruences.

Equation (13) is very useful to analyze the contributions to the vorticity because the electromagnetic and mass current terms can be easily identified there. Moreover, this identification can be accompanied by further expressing these contributions in terms of the parameters of the Ernst potentials (3). In particular, in absence of electromagnetic fields, the imaginary part of $\mathcal{E}$ is associated with mass currents. Thus, for static sources one could attempt to assume $\mathcal{E}$ as real in Eq. (13) and focus only on the electromagnetic contributions encoded in Φ. However, because $\mathcal{E}$ and Φ are not independent objects [see, e.g., Eq. (2)], in the presence of electromagnetic fields, $\mathcal{E}$ and Φ are complex even for nonspinning astrophysical objects. Notwithstanding, if Φ is purely real or purely imaginary, for nonrotating objects, the imaginary part of $\mathcal{E}$ vanishes [see, e.g., Eq. (2)]. Therefore, interest here is in identifying when the electromagnetic contribution does not vanish.

In doing so, it is convenient to express $\omega_{\rm v} = |\Im(\nabla\mathcal{E} + 2\Phi^*\nabla\Phi)|/(\sqrt{2f}e^{\gamma})$, so that the term $\Im\Phi^*\nabla\Phi$ vanishes if Φ is purely real, purely imaginary or when their real and imaginary parts are proportional to each other. Based on the discussion above [see also Eq. (5)], the purely real case corresponds to the absence of magnetic fields and the purely imaginary case to the absence of electric fields. In the cases when the Poynting vector is zero, the electromagnetic contribution to the vorticity vanishes; this generalizes the results in Ref. [6] where a particular spacetime was considered. The particular case of proportional real and imaginary parts leads to the case of proportional electric and magnetic fields and corresponds to the cases studied in Refs. [4,6].

Note that the considerations above on the vorticity scalar and the Poynting vector are completely general and valid for any stationary axially symmetric spacetime.

To study the contribution of the electromagnetic energy flux to the vorticity, characterize first the contributions of the rotation of the source. In this case, the Ernst potential Φ that encodes all the electromagnetic moments is zero and $\mathcal{E}$ is complex. For fast rotating stars, the vorticity scalar (and the Lense-Thirring effect) is larger than for slow rotating stars, this can be seen in Fig. 4.

When one includes an electromagnetic field to a particular star model, the Ernst potential Φ is no longer zero, and it has an important role in the vorticity scalar. The particular contribution depends on the structure generated by the multipole expansion and the Poynting vector. Before considering the purely electromagnetic contribution to the frame dragging in realistic situations (zero or negligible total electric charge), consider the case of a source with a dipole magnetic field and electric charge.

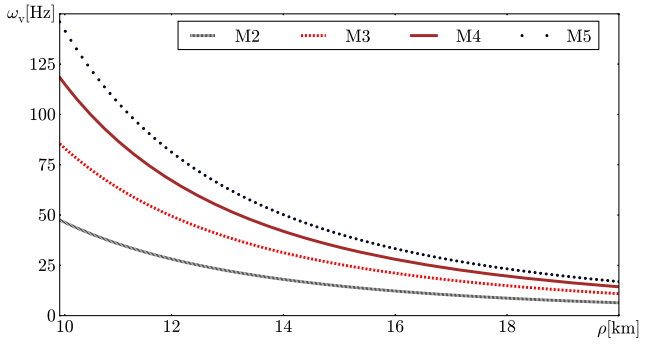

FIG. 4 (color online). Vorticity generated by the mass currents. All the electromagnetic moments are zero in this case. The vorticity of the spacetime was calculated for the models 2 ($j = 0.194$), 3 ($j = 0.324$), 4 ($j = 0.417$) and 5 ($j = 0.483$) with the equation of state L in Ref. [62]. They are listed in the Table II.

The upper panel of Fig. 5 depicts the functional dependence of the vorticity scalar on the distance from

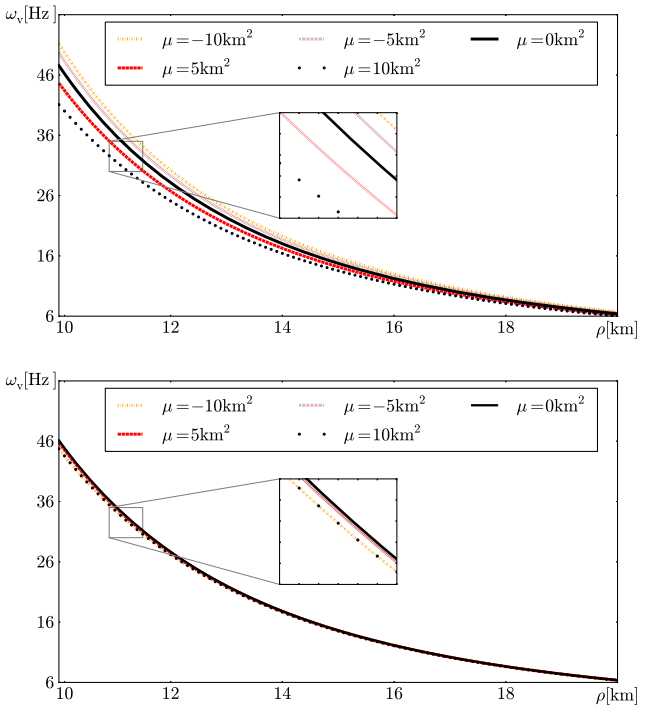

FIG. 5 (color online). Electromagnetically generated vorticity by the presence of a magnetic dipole and a fixed electric monopole of $\varsigma = 0.1$ km (upper panel with $\upsilon = 0$, $\chi = 0$ and $\zeta = 0$) and an electric dipole of $\upsilon = 10$ km^2 (lower panel with $\varsigma = 0$, $\chi = 0$ and $\zeta = 0$). The vorticity of the spacetime was calculated for model 2 for the equation of state L in Ref. [62]. Parameters are listed in Table II.

the star for a fixed value of the electric monopole and for a variety of magnetic dipole moments. The vorticity scalar decreases (increases) from its value in the vacuum situation ($\mu = 0$) when the dipole is parallel (antiparallel) to the star's rotation axis. The reason for this phenomenon can be understood in terms of Eq. (13). To do so, note that $\mathcal{E}$ decreases monotonically as a function of z and ρ; thus, its derivatives carry a negative sign. Although the same argument applies to Φ, when the sign of μ changes (see above), the Poynting vector changes its circulation and that is enough to change the sign of its contribution to the vorticity scalar [see Eq. (13)]. Alternatively, assume that the reflection symmetry exists and set the mass current parameters a and s to zero; for this case, $\Phi(\rho, z; a = 0, s = 0, -\mu) = \Phi^*(\rho, z; a = 0, s = 0, \mu)$ and therefore $\Im\Phi^*\nabla\Phi$ changes sign.

The lower panel of Fig. 5 depicts the functional dependence of the vorticity scalar on the distance from the star for a fixed value of the electric dipole and for a variety of magnetic dipole moments. The contribution in this case is weaker than in the case of an electric monopole. However, results in the lower panel of Fig. 5 are more realistic than those in the upper panel. Interestingly, in the lower panel, there is no change in the sign of the electromagnetic contribution to the vorticity scalar when μ changes sign. The reason for this relies on the fact that for $\upsilon \neq 0$ or $\zeta \neq 0$, the reflection symmetry around the equatorial plane breaks down and the arguments provided above do not apply; i.e., $\Phi(\rho, z; a = 0, s = 0, -\mu)$ does not equate to $\Phi^*(\rho, z; a = 0, s = 0, \mu)$.

Based on the processes described above on the generation of a Poynting vector from the fields induced by the mass currents ($a \neq 0$ and $s \neq 0$), it is clear that even if the parameters associated with the electric field (ς, υ and χ) are set to zero, but the parameters associated with the magnetic field (μ and ζ) are nonvanishing, then a rotationally induced electromagnetic contribution to the vorticity scalar is present. A similar scenario takes place if the parameters associated with the magnetic field are set to zero and nonvanishing electric parameters are considered. In particular, even in the low rotation regime, a non-negligible electric field is generated [64] and may be important to characterize the evolution of the electromagnetic structure in neutron stars. Moreover, in the case of fast rotation, the frame dragging caused by a Kerr black hole significantly distorts the structure of an external magnetic field and this scenario may be relevant for low accreting black holes as the one present in the Milky Way center [65,66].

The most relevant contributions to the vorticity scalar from the electromagnetic field were considered above. However, in general, all the multipole moments contribute to the vorticity scalar and the details of the net result may deviate from those discussed above; albeit, the magnitude of the effect is not expected to differ from the predictions in Fig. 5.

VI. ORBITAL EQUATORIAL MOTION AND EPICYCLIC FREQUENCIES

In general relativity, as in Newtonian gravitation, all the physical characteristics of the source have an effect on the dynamics of orbiting of particles. One of the most distinctive points between both theories is the frame dragging, but is not an observable by itself. A way to measure it is to appeal to the dynamics around the source and characterize the behavior of, e.g., neutral test particles [40,53].

Observationally, the Keplerian motion of matter could be useful to model the quasiperiodic oscillations (QPOs) that are present in the LMXBs containing a neutron star [67]. These oscillations occur at frequencies in the range of kHz and come in pairs; the upper and the lower mode correspond to the frequencies of Keplerian motion and periastron precession of the accreted matter in the close vicinity of the star [52]. An additional effect is that these equatorial orbits will exhibit a relativistic nodal precession due to frame dragging [53], causing a detectable signal in the spectra of LMXBs [68].

The following subsections are devoted to quantifying the magnetic quadrupole effect in the innermost stable circular orbit (ISCO) and the epicyclic frequencies for different models of neutron stars [62].

A. Influence of the field on the ISCO radii

The dynamics of an orbiting particle can be analyzed by using the Lagrangian formalism. To do so, consider a particle of rest mass $\mathfrak{m}_0 = 1$ moving in the spacetime described by the metric functions in Eq. (1); the Lagrangian of the particle is then given by

$$\mathcal{L} = \frac{1}{2} g_{\mu\nu} \dot{x}^\mu \dot{x}^\nu, \tag{14}$$

where the dot denotes differentiation with respect to the proper time τ, and $x^\mu(\tau)$ are the Weyl-Lewis-Papapetrou coordinates. For a stationary and axisymmetric spacetime, there are two constants of motion related to the time coordinate t and azimuthal coordinate ϕ. Thus, the energy and the canonical angular momentum, respectively, are conserved (see Ref. [69] for details). Assuming that the motion takes place in the equatorial plane of the star $z = 0$, and taking into account the four velocity normalization for massive particles $g_{\mu\nu} u^\mu u^\nu = -1$, one can identify an effective potential that characterizes the motion in the plane (see, e.g., Ref. [70])

$$V_{\text{eff}}(\rho) = 1 - \frac{E^2 g_{\phi\phi} + 2EL g_{t\phi} + L^2 g_{tt}}{g_{t\phi}^2 - g_{\phi\phi} g_{tt}}. \tag{15}$$

For a particle moving in a circular orbit, the energy E and the canonical angular momentum L are determined by the conditions $V_{\text{eff}}(\rho) = 0$ and $\mathrm{d}V_{\text{eff}}/\mathrm{d}\rho = 0$ (see, e.g.,

Ref. [71]). The marginal stability condition reads $d^2V_{\rm eff}/d\rho^2 = 0$. Thus, the ISCO's radius is determined by solving numerically the previous equation for ρ.

The importance of determining the ISCO is that accretion disks extend from the last stable orbit to exterior zones, so the ISCO is an inner boundary for the accreted matter. As stated above, the inclusion of a magnetic field causes a dependence of all physical quantities of the intensity on the field. From the International System of Units (SI), the conversion to geometrized units is given by

$$\mu_{\rm geom} = \frac{10^{-6}\sqrt{G\mu_0}}{c^2}\mu_{\rm SI}, \tag{16}$$

where G is the gravitational constant, μ_0 is the vacuum permittivity, c is the speed of light and μ is given in units of Am^2. The units of ζ are Am^3 and the conversion for the quadrupole reads

$$\zeta_{\rm geom} = \frac{10^{-9}\sqrt{G\mu_0}}{c^2}\zeta_{\rm SI}. \tag{17}$$

In the same way, the electric multipole moments can be written in geometrized units as

$$\varsigma_{\rm geom} = \sqrt{\frac{G\mu_0}{4\pi}}\varsigma_{\rm SI}, \tag{18}$$

$$\upsilon_{\rm geom} = 10^{-3}\sqrt{\frac{G\mu_0}{4\pi}}\upsilon_{\rm SI}, \tag{19}$$

$$\chi_{\rm geom} = 10^{-6}\sqrt{\frac{G\mu_0}{4\pi}}\varsigma_{\rm SI}. \tag{20}$$

Consider a superposition of a fixed dipolar and quadrupole component that will be varied from 1 to 50 km^3. Figure 6 depicts the ISCO radius as a function of the parameter μ and ζ for three realistic numerical solutions for rotating neutron stars models derived in Ref. [62]. The parameter μ is set to 1 km^2 that corresponds to a magnetic dipole field of 10^{12} T. The quadrupole parameter ζ is chosen between 0 and 50 km^3 that corresponds to magnetic quadrupoles from 0 to 5×10^{35} Am^3, respectively. In all these cases, the ISCO radius decreases for increasing ζ. This can be explained as a result of the deformation of the spacetime by the energy stored in the electromagnetic (see, e.g., Ref. [40]). We elaborate more on this in the next section.

B. Influence of the electromagnetic field in the Keplerian and the epicyclic frequencies

Imposing the conditions of constant orbital radius, $d\rho/d\tau = 0$, and taking into account that $d\phi/d\tau = \Omega_{\rm K}dt/d\tau$, the Keplerian frequency reads (see, e.g., Ref. [69])

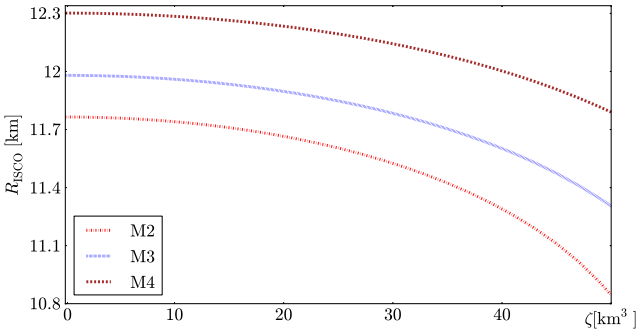

FIG. 6 (color online). ISCO radius as a function of magnetic quadrupole parameter ζ, with $\mu = 0$ km^2. The physical parameters for the star correspond to the models 2–4 listed in Table II. We can see that the ISCO radius decreases for increasing ζ.

$$\Omega_{\rm K} = \frac{d\phi}{dt} = \frac{-g_{t\phi,\rho} \pm \sqrt{(g_{t\phi,\rho})^2 - g_{\phi\phi,\rho}g_{tt,\rho}}}{g_{\phi\phi,\rho}}, \tag{21}$$

where "+" and "−" denote the Keplerian frequency for corotating and counterrotating orbits, respectively. In Ref. [40] the functional dependence of the Keplerian frequency on the magnetic dipole parameter μ was discussed; here interest is in the functional dependence on the magnetic quadrupole parameter ζ. The upper panel of Fig. 7 depicts the functional dependence on ζ, as in the case analyzed in Ref. [40], the Keplerian frequency increases with increasing ζ because the ISCO's radius decreases (see Fig. 6) as a consequence of the additional deformation of the spacetime by the electromagnetic field. In particular, the energy of the electromagnetic field shifts the marginally unstable region toward the star.

Analytical expressions for the radial and vertical frequencies follow from allowing slightly radial and vertical perturbations of the orbit. According to Ref. [69], the radial and vertical epicyclic frequencies are given by

$$\begin{aligned}\nu_\alpha = \frac{1}{2\pi}\Bigg\{-\frac{g^{\alpha\alpha}}{2}\Bigg[&(g_{tt}+g_{t\phi}\Omega_k)^2\left(\frac{g_{\phi\phi}}{\rho^2}\right)_{,\alpha\alpha}\\ &-2(g_{tt}+g_{t\phi}\Omega_k)(g_{t\phi}+g_{\phi\phi}\Omega_k)\left(\frac{g_{t\phi}}{\rho^2}\right)_{,\alpha\alpha}\\ &+(g_{t\phi}+g_{\phi\phi}\Omega_k)^2\left(\frac{g_{tt}}{\rho^2}\right)_{,\alpha\alpha}\Bigg]\Bigg\},\end{aligned} \tag{22}$$

with $\alpha = \{\rho, z\}$. In the relativistic precession model (RPM) [51], the periastron $\nu_\rho^{\rm p}$ and the nodal $\nu_z^{\rm p}$ frequencies are the observationally relevant ones; they are defined by

$$\nu_\alpha^{\rm p} = \frac{\Omega_{\rm K}}{2\pi} - \nu_\alpha. \tag{23}$$

At the ISCO, the radial oscillation frequency equals the Keplerian frequency and only the vertical precession $\alpha = z$

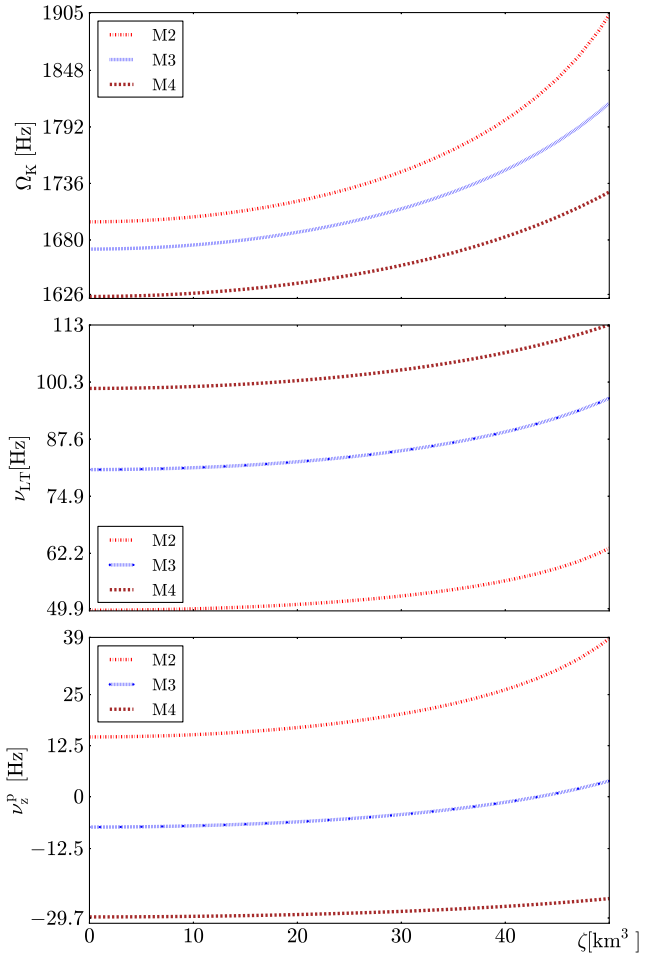

FIG. 7 (color online). Influence of the magnetic quadrupole moment ζ in the epicyclic frequencies for different models of neutron stars with $\varsigma = 0$, $\mu = 1$ km^2, $\upsilon = 0$ and $\chi = 0$. Vacuum parameters of the star are listed in Table II.

is considered here. The influence of the magnetic quadrupole on the vertical precession frequency is depicted in the lower panel of Fig. 7. The behavior and the underlying physical mechanism are analogous to those for the Keplerian frequency.

The frequency $\nu_{\rm LT}$ that characterizes the Lense-Thirring effect is given by (see, e.g., Ref. [69])

$$\nu_{\rm LT} = -\frac{1}{2\pi}\frac{g_{t\phi}}{g_{\phi\phi}}, \tag{24}$$

and could be relevant to model the horizontal branch oscillations observed in the LMXBs [51]. The strength of the frame-dragging effect increases for fast rotating objects and, as shown in the central panel of Fig. 7, for stronger magnetic fields. Figure 7 also shows that the electromagnetically induced frame dragging has a direct effect on the orbiting particles, even if they are neutral.

VII. CONCLUDING REMARKS

We present a new stationary axisymmetric nine-parameter closed-form analytic solution that generalizes the Kerr solution with arbitrary mass-quadrupole moment, octupole current moment, electric and magnetic dipole and electric and magnetic quadrupole moments. The analytic form of its multipolar structure and their electric and magnetic fields are also presented. According to the arguments presented through the paper, this solution could be used to model the exterior gravitational and electromagnetic fields around strongly magnetized stars, in particular white dwarfs. Also, this model could be used even for the description of exotic stars such as the τ Sco recently reported by Donati *et al.* [72].

This solution allowed for a comprehensive analysis of the contribution of complex and intense electromagnetic fields to a quintessential hallmark of general relativity, namely, the Lense-Thirring effect. It was shown that if the value of the parameters is such that the reflection symmetry is preserved [49], then a sign change of the magnetic dipole parameter μ is enough to change the direction of the circulation of the Poynting vector and the sign of the electromagnetic contribution to the vorticity scalar. The influence of complex electromagnetic fields on the ISCO's radius and the epicyclic frequencies were also considered and it was shown that for strong magnetic fields, the influence is not negligible.

Additional interest is in studying the effect of the magnetic field in the quadrupole moment of the star (see, e.g., Refs. [73,74]). This topic has gained recently theoretical and observational interest and is currently discussed under the title of I-Love-Q relations [74]. Due to the great generality of the present analytic exact solution, this subject will be explored in a forthcoming contribution [75].

ACKNOWLEDGMENTS

Fruitful discussions with Prof. César A. Valenzuela-Toledo are acknowledged with pleasure. This work was partially supported by Fundación para la Promoción de la Investigación y la Tecnología del Banco la República Grant No. 2879. and by Comité para el Desarrollo de la Investigación (CODI) of Universidad de Antioquia under the Estrategia de Sostenibilidad 2015-2016.

APPENDIX A: METRIC FUNCTIONS OF THE DEVELOPED SOLUTION

This appendix summarizes the relevant equations of the developed metric. The potentials in the symmetry axis can be written as [54]

$$e(z) = 1 + \sum_{i=3}^{3} \frac{e_i}{z-\beta_i}, \qquad f(z) = \sum_{i=3}^{3} \frac{f_i}{z-\beta_i}, \tag{A1}$$

with

$$e_j = (-1)^j \frac{2m\beta_j^2}{(\beta_j-\beta_k)(\beta_j-\beta_i)},$$
$$f_j = \frac{i\zeta + (\varsigma + i\mu)\beta_j}{(\beta_j-\beta_k)(\beta_j-\beta_i)}, \qquad i,k \neq j. \tag{A2}$$

Then, the Ernst potentials and the metric functions in whole spacetime are derived with the aid of Sibgatullin's integral method [47,48]. By using the representation proposed in Ref. [76] and used also in Ref. [42],

$$\mathcal{E} = \frac{A+B}{A-B}, \qquad \Phi = \frac{C}{A-B},$$
$$f = \frac{A\bar{A} - B\bar{B} + C\bar{C}}{(A-B)(\bar{A}-\bar{B})}, \qquad e^{2\gamma} = \frac{A\bar{A} - B\bar{B} + C\bar{C}}{K\bar{K}\prod_{n=1}^{6} r_n},$$
$$\omega = \frac{\mathrm{Im}[(A+B)\bar{H} - (\bar{A}+\bar{B})G - C\bar{I}]}{A\bar{A} - B\bar{B} + C\bar{C}}, \tag{A3}$$

where

$$A = \sum_{1\le i<j<k\le 6} a_{ijk} r_i r_j r_k, \qquad B = \sum_{1\le i<j\le 6} b_{ij} r_i r_j, \qquad C = \sum_{1\le i<j\le 6} c_{ij} r_i r_j, \qquad K = \sum_{1\le i<j<k\le 6} a_{ijk},$$
$$H = zA - (\beta_1+\beta_2+\beta_3)B + \sum_{1\le i<j<k\le 6} h_{ijk} r_i r_j r_k + \sum_{1\le i<j\le 6} (\alpha_i+\alpha_j) b_{ij} r_i r_j,$$
$$G = -(\beta_1+\beta_2+\beta_3)A + zB + \sum_{1\le i<j\le 6} g_{ij} r_i r_j + \sum_{1\le i<j<k\le 6} (\alpha_i+\alpha_j+\alpha_k) a_{ijk} r_i r_j r_k,$$
$$I = (f_1+f_2+f_3)(A-B) + (\beta_1+\beta_2+\beta_3 - z)C + \sum_{1\le i<j<k\le 6} p_{ijk} r_i r_j r_k + \sum_{i=1}^{6} p_i r_i + \sum_{1\le i<j\le 6} [p_{ij} - (\alpha_i+\alpha_j)c_{ij}] r_i r_j,$$

with

$$r_i = \sqrt{\rho^2 + (z-\alpha_i)^2}, \qquad a_{ijk} = (-1)^{i+j+1}\Lambda_{ijk}\Gamma_{l|mn}, \qquad b_{ij} = (-1)^{i+j}\lambda_{ij} H_{l|mnp},$$
$$c_{ij} = (-1)^{i+j}\lambda_{ij}[f(\alpha_l)\Gamma_{m|np} - f(\alpha_m)\Gamma_{n|pl} + f(\alpha_n)\Gamma_{p|lm} - f(\alpha_p)\Gamma_{l|mn}],$$
$$h_{ijk} = (-1)^{i+j+k}\Lambda_{ijk}(e_1^* \delta_{23|lmn} + e_2^* \delta_{31|lmn} + e_3^* \delta_{12|lmn}),$$
$$g_{ij} = (-1)^{i+j}\lambda_{ij}(\alpha_l\Gamma_{m|np} - \alpha_m\Gamma_{n|pl} + \alpha_n\Gamma_{p|lm} - \alpha_p\Gamma_{l|mn}),$$
$$p_i = (-1)^i D_i[f(\alpha_l)H_{m|nps} - f(\alpha_m)H_{n|psl} + f(\alpha_n)H_{p|slm} - f(\alpha_p)H_{s|lmn} + f(\alpha_s)H_{l|mnp}],$$
$$p_{ij} = (-1)^{i+j}\lambda_{ij}(e_1^*\Upsilon_{23|lmnp} + e_2^*\Upsilon_{31|lmnp} + e_3^*\Upsilon_{12|lmnp}),$$
$$p_{ijk} = (-1)^{i+j+1}\Lambda_{ijk}(e_1^*\Psi_{23|lmn} + e_2^*\Psi_{31|lmn} + e_3^*\Psi_{12|lmn}),$$

and

$$\lambda_{ij} = (\alpha_i-\alpha_j)D_iD_j, \qquad \Lambda_{ijk} = (\alpha_i-\alpha_j)(\alpha_i-\alpha_k)(\alpha_j-\alpha_k)D_iD_jD_k, \qquad D_i = \frac{1}{(\alpha_i-\beta_1)(\alpha_i-\beta_2)(\alpha_i-\beta_3)},$$
$$\Gamma_{l|mn} = H_3(\alpha_l)\Delta_{12|mn} + H_3(\alpha_m)\Delta_{12|nl} + H_3(\alpha_n)\Delta_{12|lm}, \qquad \Delta_{lm|np} = H_l(\alpha_n)H_m(\alpha_p) - H_l(\alpha_p)H_m(\alpha_n),$$
$$H_l(\alpha_n) = \frac{2\prod_{p\neq n}(\alpha_p - \beta_l^*)}{\prod_{k\neq l}^{3}(\beta_l^* - \beta_k^*)\prod_{k=1}^{3}(\beta_l^* - \beta_k)} - 2\sum_{k=1}^{3}\frac{f_l^* f_k}{(\beta_l^* - \beta_k)(\alpha_n - \beta_k)}, \qquad \delta_{lm|nps} = \Delta_{lm|np} + \Delta_{lm|ps} + \Delta_{lm|sn},$$
$$h_{l|mnp} = H_3(\alpha_l)\delta_{12|mnp}, \qquad H_{l|mnp} = h_{l|mnp} + h_{m|npl} + h_{n|plm} + h_{p|lmn},$$
$$\Psi_{lm|nps} = f(\alpha_n)\Delta_{lm|ps} + f(\alpha_p)\Delta_{lm|sn} + f(\alpha_s)\Delta_{lm|np},$$
$$\Upsilon_{lm|nprs} = f(\alpha_n)\delta_{lm|prs} - f(\alpha_p)\delta_{lm|rsn} + f(\alpha_r)\delta_{lm|snp} - f(\alpha_s)\delta_{lm|npr},$$

α's being the roots of Sibgatullin's equation [47,48]

$$e(z)+\tilde{e}(z)+2\tilde{f}(z)f(z)=0. \tag{A4}$$

APPENDIX B: ELECTROMAGNETIC FIELD: ANALYTIC FORM

The A_t potential is the real part of the electromagnetic Ernst potential Φ, and the potential A_ϕ can be calculated as the real part of the Kinnersley potential $\mathcal{K}=A_\phi+iA'_t$ [77], which can be obtained using Sibgatullin's method and can be written as

$$\mathcal{K}=-i\frac{I(f_1+f_2)}{A-B}. \tag{B1}$$

Thus, the closed-form expressions for the electric and magnetic fields are

$$E_\rho=-\frac{\Lambda}{\sqrt{|A|^2-|B|^2+|C|^2}}\mathrm{Re}\left\{\left[\frac{C_{,\rho}-C\ln(A-B)_{,\rho}}{A-B}\right]\right\},$$

$$E_z=-\frac{\Lambda}{\sqrt{|A|^2-|B|^2+|C|^2}}\mathrm{Re}\left\{\left[\frac{C_{,z}-C\ln(A-B)_{,z}}{A-B}\right]\right\},$$

$$B_\rho=\frac{\mathrm{Im}(A-B)\bar{H}+(\bar{A}-\bar{B})G-C\bar{I}]}{\rho|A-B|^2}E_z+\frac{\Lambda\sqrt{|A|^2-|B|^2+|C|^2}}{\rho|A-B|^2}\mathrm{Im}\times\left\{\frac{(\bar{f}_1+\bar{f}_2)[\bar{I}_{,z}-\bar{I}\ln(\bar{A}-\bar{B})_{,z}]}{A-B}\right\},$$

$$B_z=-\frac{\mathrm{Im}(A-B)\bar{H}+(\bar{A}-\bar{B})G-C\bar{I}]}{\rho|A-B|^2}E_\rho+\frac{\Lambda\sqrt{|A|^2-|B|^2+|C|^2}}{\rho|A-B|^2}\mathrm{Im}\times\left\{\frac{(\bar{f}_1+\bar{f}_2)[\bar{I}_{,\rho}-\bar{I}\ln(\bar{A}-\bar{B})_{,\rho}]}{A-B}\right\}.$$

when

$$\Lambda=\frac{|K|^2\prod_{n=1}^{6}r_n}{|A-B|}.$$

[1] C. Everitt *et al.*, Phys. Rev. Lett. **106**, 221101 (2011).
[2] C. Chakraborty and P. Pradhan, Eur. Phys. J. C **73**, 2536 (2013).
[3] C. Chakraborty and P. Majumdar, Classical Quantum Gravity **31**, 075006 (2014).
[4] A. Das, J. Math. Phys. (N.Y.) **20**, 740 (1979).
[5] W. Bonnor, Phys. Lett. A **158**, 23 (1991).
[6] L. Herrera, G. A. Gonzalez, L. A. Pachón, and J. A. Rueda, Classical Quantum Gravity **23**, 2395 (2006).
[7] V. S. Manko, E. D. Rodchenko, B. I. Sadovnikov, and J. Sod-Hoffs, Classical Quantum Gravity **23**, 5389 (2006).
[8] L. Herrera and W. Barreto, Phys. Rev. D **86**, 064014 (2012).
[9] L. Herrera, Gen. Relativ. Gravit. **46**, 1654 (2013).
[10] M. S. Bhatia, S. Bonazzola, and G. Szamosi, Astron. Astrophys. **3**, 206 (1969).
[11] P. Ghosh and F. K. Lamb, Astrophys. J. Lett. **223**, L83 (1978).
[12] P. Ghosh and F. K. Lamb, Astrophys. J. **232**, 259 (1979).
[13] M. Camenzind, in *Reviews in Modern Astronomy* Vol. 3, edited by G. Klare (Springer, Berlin Heidelberg, 1990), pp. 234–265.
[14] A. Koenigl, Astrophys. J. Lett. **370**, L39 (1991).
[15] M. M. Romanova, G. V. Ustyugova, A. V. Koldoba, and R. V. E. Lovelace, Astrophys. J. **578**, 420 (2002).
[16] M. M. Romanova, G. V. Ustyugova, A. V. Koldoba, J. V. Wick, and R. V. E. Lovelace, Astrophys. J. **595**, 1009 (2003).
[17] M. M. Romanova, G. V. Ustyugova, A. V. Koldoba, and R. V. E. Lovelace, Astrophys. J. **610**, 920 (2004).
[18] M. Long, M. M. Romanova, and R. V. E. Lovelace, Astrophys. J. **634**, 1214 (2005).
[19] W. Becker, *Neutron Stars and Pulsars*, Astrophysics and Space Science Library (Springer, New York, 2009).
[20] T. Güver, E. Göğüş, and F. Özel, Mon. Not. R. Astron. Soc. **418**, 2773 (2011).
[21] S. V. Berdyugina, Living Rev. Solar Phys. **2**, 8 (2005).
[22] J.-F. Donati and A. Collier Cameron, Mon. Not. R. Astron. Soc. **291**, 1 (1997).
[23] J.-F. Donati, A. Collier Cameron, G. A. J. Hussain, and M. Semel, Mon. Not. R. Astron. Soc. **302**, 437 (1999).
[24] M. Jardine, K. Wood, A. Collier Cameron, J.-F. Donati, and D. H. Mackay, Mon. Not. R. Astron. Soc. **336**, 1364 (2002).
[25] M. Jardine, A. C. Cameron, J.-F. Donati, S. G. Gregory, and K. Wood, Mon. Not. R. Astron. Soc. **367**, 917 (2006).
[26] C. P. Johnstone and M. Jardine, S. G. Gregory, J.-F.Donati, and G. Hussain, arXiv:1310.8194v1.
[27] I. Appenzeller and R. Mundt, Astron. Astrophys. Rev. **1**, 291 (1989).
[28] J.-F. Donati, M. M. Jardine, S. G. Gregory, P. Petit, J. Bouvier, C. Dougados, F. Ménard, A. Collier Cameron, T. J. Harries, S. V. Jeffers, and F. Paletou, Mon. Not. R. Astron. Soc. **380**, 1297 (2007).
[29] G. D. Schmidt *et al.*, Astrophys. J. **595**, 1101 (2003).
[30] K. M. Vanlandingham, G. D. Schmidt, D. J. Eisenstein, H. C. Harris, S. F. Anderson, P. B. Hall, J. Liebert, D. P.

Schneider, N. M. Silvestri, G. S. Stinson, and M. A. Wolfe, Astrophys. J. **130**, 734 (2005).
[31] S. J. Kleinman, S. O. Kepler, D. Koester, I. Pelisoli, V. Peanha, A. Nitta, J. E. S. Costa, J. Krzesinski, P. Dufour, F.-R. Lachapelle, P. Bergeron, C.-W. Yip, H. C. Harris, D. J. Eisenstein, L. Althaus, and A. Crsico, Astrophys. J. Suppl. Ser. **204**, 5 (2013).
[32] K. Beuermann, F. Euchner, K. Reinsch, S. Jordan, and B. T. Gnsicke, Astron. Astrophys. **463**, 647 (2007).
[33] S. Jordan, R. Aznar Cuadrado, R. Napiwotzki, H. M. Schmid, and S. K. Solanki, Astron. Astrophys. **462**, 1097 (2007).
[34] F. Euchner, S. Jordan, K. Reinsch, K. Beuermann, and B. T. Gänsicke, in *14th European Workshop on White Dwarfs*, Astronomical Society of the Pacific Conference Series, Vol. 334, edited by D. Koester and S. Moehler (Astronomical Society of the Pacific, San Francisco, 2005), p. 269.
[35] G. Landstreet and J. D. Mathys, Astron. Astrophys. **359**, 213 (2000).
[36] S. Olausen and M. Kaspi, Astrophys. J. Suppl. Ser. **212**, 6 (2014).
[37] S. Mereghetti, Astron. Astrophys. Rev. **15**, 225 (2008).
[38] N. Rea *et al.*, Astrophys. J. **770**, 65 (2013).
[39] T. Güver, E. Göğüş, and F. Özel, Mon. Not. R. Astron. Soc. **418**, 2773 (2011).
[40] A. F. Gutiérrez-Ruiz, L. A. Pachón, and C. A. Valenzuela-Toledo, Universitas Scientiarum **19**, 63 (2013).
[41] L. A. Pachón, J. A. Rueda, and C. A. Valenzuela-Toledo, Astrophys. J. **756**, 82 (2012).
[42] L. A. Pachón, J. A. Rueda, and J. D. Sanabria-Gómez, Phys. Rev. D **73**, 104038 (2006).
[43] D. Bini, A. Geralico, O. Luongo, and H. Quevedo, Classical Quantum Gravity **26**, 225006 (2009).
[44] T. Johannsen and D. Psaltis, Phys. Rev. D **83**, 124015 (2011).
[45] S. Toktarbay and H. Quevedo, Gravitation Cosmol. **20**, 252 (2014).
[46] F. J. Ernst, Phys. Rev. **172**, 1850 (1968).
[47] N. R. Sibgatullin, *Oscillations and Waves in Strong Gravitational and Electromagnetic Fields*, Volume XIV (Springer-Verlag, Berlin, 1991), p. 26.
[48] V. S. Manko and N. R. Sibgatullin, Classical Quantum Gravity **10**, 1383 (1993).
[49] L. A. Pachón and J. D. Sanabria-Gómez, Classical Quantum Gravity **23**, 3251 (2006).
[50] F. J. Ernst, V. S. Manko, and E. Ruiz, Classical Quantum Gravity **23**, 4945 (2006).
[51] L. Stella and M. Vietri, Phys. Rev. Lett. **82**, 17 (1999).
[52] S. M. Morsink and L. Stella, Astrophys. J. **513**, 827 (1999).
[53] L. Stella and M. Vietri, Astrophys. J. Lett. **492**, L59 (1998).
[54] E. Ruiz, V. S. Manko, and J. Martín, Phys. Rev. D **51**, 4192 (1995).
[55] A. Papapetrou, Ann. Phys. (Berlin) **447**, 309 (1953).
[56] C. Hoenselaers and Z. Perjes, Classical Quantum Gravity **7**, 1819 (1990).
[57] T. P. Sotiriou and T. A. Apostolatos, Classical Quantum Gravity **21**, 5727 (2004).
[58] B. Werner, *Neutron Stars and Pulsars* (Springer-Verlag, Berlin Heidelberg, 2009).
[59] M. Bocquet, S. Bonazzola, E. Gourgoulhon, and J. Novak, Astron. Astrophys. **301**, 757 (1995).
[60] F. L. Dubeibe, L. A. Pachón, and J. D. Sanabria-Gómez, Phys. Rev. D **75**, 023008 (2007).
[61] R. M. Wald, *General relativity* (University of Chicago Press, Chicago, 1984).
[62] G. Pappas and T. A. Apostolatos, Phys. Rev. Lett. **108**, 231104 (2012).
[63] E. S. B. Manko, V. Rodchenko, and J. Sod-Hoffs, Classical Quantum Gravity **23**, 5389 (2006).
[64] L. Rezzolla, B. J. Ahmedov, and J. C. Miller, Mon. Not. R. Astron. Soc. **322**, 723 (2001).
[65] V. Karas, V. Kopáček, and D. Kunneriath, Classical Quantum Gravity **29**, 035010 (2012).
[66] V. Karas, O. Kopáček, and D. Kunneriath, Acta Polytech. **54**, 398 (2014).
[67] M. van der Klis, Adv. Space Res. **38**, 2675 (2006).
[68] J. Homan, Astrophys. J. Lett. **760**, L30 (2012).
[69] F. D. Ryan, Phys. Rev. D **52**, 5707 (1995).
[70] J. M. Bardeen, W. H. Press, and S. A. Teukolsky, Astrophys. J. **178**, 347 (1972).
[71] M. Stute and M. Camenzind, Mon. Not. R. Astron. Soc. **336**, 831 (2002).
[72] J.-F. Donati, I. D. Howarth, M. M. Jardine, P. Petit, C. Catala, J. D. Landstreet, J.-C. Bouret, E. Alecian, J. R. Barnes, T. Forveille, F. Paletou, and N. Manset, Mon. Not. R. Astron. Soc. **370**, 629 (2006).
[73] A. Mastrano, P. D. Lasky, and A. Melatos, Mon. Not. R. Astron. Soc. **434**, 1658 (2013).
[74] B. Haskell, R. Ciolfi, F. Pannarale, and L. Rezzolla, Mon. Not. R. Astron. Soc. **438**, L71 (2014).
[75] A. Gutierrez-Ruiz, C. Valenzuela-Toledo, and L. A. Pachon (to be published).
[76] N. Bretón, V. S. Manko, and J. Aguilar Sánchez, Classical Quantum Gravity **16**, 3725 (1999).
[77] W. Kinnersley, J. Math. Phys. (N.Y.) **18**, 1529 (1977).